HHS Public Access

Author manuscript

Mol Cancer Ther. Author manuscript; available in PMC 2021 June 16.

Published in final edited form as:

Mol Cancer Ther. 2020 December ; 19(12): 2465–2475. doi:10.1158/1535-7163.MCT-20-0271.

Glutaminase inhibitors induce thiol-mediated oxidative stress and radio-sensitization in treatment resistant cervical cancers

Ramachandran Rashmi[1], **Kay Jayachandran**[1], **Jin Zhang**[1,2], **Vishnu Menon**[1,3], **Naoshad Muhammad**[1], **Michael Zahner**[1], **Fiona Ruiz**[1], **Sisi Zhang**[4], **Kevin Cho**[4], **Yuting Wang**[4], **Xiaojing Huang**[5], **Yi Huang**[1], **Michael L. McCormick**[6], **Buck E. Rogers**[1], **Douglas R. Spitz**[6], **Gary J. Patti**[4,7], **Julie K. Schwarz**[1,8,9]

[1]Department of Radiation Oncology, Washington University School of Medicine, St. Louis, Missouri.

[2]Institute for Informatics, Washington University School of Medicine, St. Louis, Missouri.

[3]School of Biotechnology, Amrita Vishwa Vidyapeetham, Kollam, India.

[4]Department of Chemistry, Washington University School of Medicine, St. Louis, Missouri.

[5]Department of Radiation Oncology, Memorial Sloan Kettering Cancer Center, New York, New York.

[6]Free Radical and Radiation Biology Program, Department of Radiation Oncology, Holden Comprehensive Cancer Center, University of Iowa, Iowa City, Iowa.

[7]Department of Medicine, Washington University School of Medicine, St. Louis, Missouri.

[8]Department of Cell Biology and Physiology, Washington University School of Medicine, St. Louis, Missouri.

[9]Alvin J. Siteman Center, Washington University School of Medicine, St. Louis, Missouri

Abstract

The purpose of the study was to determine if radiation resistant cervical cancers are dependent upon glutamine metabolism driven by activation of the PI3K pathway and test whether PI3K pathway mutation predicts radio-sensitization by inhibition of glutamine metabolism. Cervical cancer cell lines with and without PI3K pathway mutations, including SiHa and SiHa PTEN$^{-/-}$ cells engineered by CRISPR/Cas9, were used for mechanistic studies performed *in vitro* in the presence and absence of glutamine starvation and the glutaminase inhibitor, telaglenastat (CB-839). These studies included cell survival, proliferation, quantification of oxidative stress parameters, metabolic tracing with stable isotope labeled substrates, metabolic rescue and combination studies with L-buthionine sulfoximine (BSO), auranofin (AUR), and radiation (RT). *In vivo* studies of telaglenastat ± RT were performed using CaSki and SiHa xenografts grown in immune compromised mice. PI3K activated cervical cancer cells were selectively sensitive to glutamine deprivation through a mechanism that included thiol-mediated oxidative stress.

Corresponding Author: Julie Schwarz, MD, PhD, **Address:** Department of Radiation Oncology; Washington University School of Medicine, 4511 Forest Park Avenue, Saint Louis, MO 63108, **Phone:** 314-273-0275, **FAX:** 314-747-5498, jschwarz@wustl.edu.

Conflicts of Interest: The authors declare no potential conflicts of interest.

Telaglenastat treatment decreased total glutathione pools, increased the percent glutathione disulfide, and caused clonogenic cell killing that was reversed by treatment with the thiol antioxidant, N-acetylcysteine. Telaglenastat also sensitized cells to killing by glutathione depletion with BSO, thioredoxin reductase inhibition with AUR, and RT. Glutamine dependent PI3K activated cervical cancer xenografts were sensitive to telaglenastat monotherapy, and telaglenastat selectively radio-sensitized cervical cancer cells *in vitro* and *in vivo*. These novel preclinical data support the utility of telaglenastat for glutamine dependent radio-resistant cervical cancers and demonstrate that PI3K pathway mutations may be used as a predictive biomarker for telaglenastat sensitivity.

Keywords

cervix; glutamine; radiation; telaglenastat

Introduction

Despite recent advances in screening and prevention, cervical cancer remains the fourth most common cancer diagnosis worldwide in women and a leading cause of cancer related mortality (1, 2). The standard of care (SOC) treatment for locally advanced cervical cancer (LACC), pelvic irradiation with concurrent administration of cisplatin chemotherapy (CRT), has not changed in more than 30 years, and clinical outcomes have stagnated (3, 4). One third of cervical cancer patients with LACC will fail SOC CRT and, although patient survival can be increased by salvage surgery or treatment with cisplatin and bevacizumab, there is currently no cure for metastatic or recurrent disease (5–7). Thus, the development of new biomarkers and treatment strategies, particularly for radiation resistant LACC, is an unmet need.

The majority of cervical cancers are Human Papillomavirus (HPV) positive, and persistent expression of HPV related oncogenes E6 and E7 is necessary but not sufficient for tumorigenesis (8–10). The most common recurrent oncogenic mutations in cervical occur within the PI3K pathway, which is mutated in 40% of cervical cancers, and results in activation of AKT and mTOR (11). Previous studies demonstrated patients with cervical cancers harboring PI3K pathway mutations are resistant to SOC CRT, but alternative approaches have yet to reach the clinic (12–16). In addition to genomics, imaging metrics, particularly high tumor glucose uptake on pretreatment ^{18}F-fluoro-deoxyglucose positron emission tomography (FDG-PET) imaging, have been used to predict poor outcomes after SOC CRT in LACC (17–20), suggesting that tumor metabolism may be an effective target. Our group has recently reported combined inhibition of glucose and redox metabolic pathways in preclinical models of radiation resistant cervical cancers (21). Challenges in the clinical translation of these results include the need for a three-drug regimen, limited availability of targeted inhibitors of tumor glycolysis, and systemic toxicities associated with inhibition of glucose metabolism.

Cancers that exhibit high rates of glucose metabolism frequently depend upon exogenous glutamine. Glutamine is used by glycolytic cancer cells for energy production, to maintain

redox homeostasis, and to generate other biosynthetic intermediates needed for cell growth (22). Inhibiting glutamine metabolism is an effective treatment strategy particularly for mTOR activated cancers that depend upon glutamine for tumor cell survival (23–26). This approach has become more attractive clinically with the recent development of an orally bioavailable inhibitor of glutaminase, telaglenastat (CB-839), that is currently being tested in clinical trials alone and in combination with other agents (25–27). The purpose of the current study was to test whether radio-resistant cervical cancers are dependent upon glutamine metabolism, and to determine the sensitivity of cervical cancer to single agent and combination therapy with telaglenastat. As there are currently no reliable predictive biomarkers for telaglenastat response, a secondary goal was to determine whether metabolic reprogramming driven by PI3K pathway mutation predicts sensitivity of cervical cancer to telaglenastat.

Materials and Methods

Cell culture and Reagents

Cervical cancer cell lines CaSki, SiHa, and C33A were obtained from the American Type Culture Collection (ATCC) and maintained in IMDM media (Life Technologies, CA) with 10% heat inactivated FBS. HCvEpC were cultured in HCvEpC media from Cell Applications, Inc. (San Diego, CA). Mycoplasma testing was performed every 3 months to verify no contamination. Last date of mycoplasma testing for cell lines used in this study was January 20, 2020. Experiments were performed on all cell lines between passages 10 and 30. SiHa PTEN$^{-/-}$ cells were generated by CRISPR nuclease-induced targeted double strand break at the Genome Engineering Center at Washington University School of Medicine (St. Louis, MO). Approximately 1×10^6 single cells were washed and re-suspended in buffer with 1 μg gRNA (5’ AACTTGTCTTCCCGTCGTGT 3’), 1.5 μg Cas9 and 0.5 μg GFP expression construct then electroporated via 4D-Nucleofector (Lonza) using EN-158 program. Single cell clones were screened for genetic knock-out genotype using targeted deep sequencing analysis (28).

L-buthionine-sulfoximine (BSO), auranofin (AUR), N-acetylcysteine (NAC), protease and phosphatase inhibitor cocktails were purchased from Sigma (Saint Louis, MO). Telaglenastat was obtained from Calithera Biosciences, Inc. (South San Francisco, CA). Telaglenastat and AUR were dissolved and diluted in dimethyl sulfoxide (DMSO) 0.002% and 0.01% respectively. BSO was dissolved in normal saline. NAC was dissolved in 10% sodium bicarbonate solution.

Cell viability and clonogenic cell survival assays

Cell viability was assessed using Cell Titre (Promega). For CB-839 and redox inhibitor experiments, cells were treated with telaglenastat 200 nM, AUR 25 nM, and BSO 125 μM for 96 hours and then plated for clonogenic assay. For NAC rescue experiments, cells were treated with CB-839 (200nM) for 72 hours followed by 7 hours of 10mM NAC and after which fresh media was added to all the treatment groups for 24 hours and then plated for clonogenic assay. For RT sensitization cells were pre-treated with telaglenastat (500nM) for 48 hours, then irradiated using an RS2000 160kV X-ray Irradiator using a 0.3 mm copper

filter (Rad Source Technologies, Suwanee, GA) and 48 hours post radiation cells were harvested and plated for clonogenic assay. After 10 days, colonies were counted after staining with crystal violet. Assays were performed in triplicate and repeated 3 times. Clonogenic survival data were fitted using the Linear-Quadratic formula. T-test was performed on the average of the three biological replicates for Dose Modifying Factors.

Analysis of whole transcriptome data

RNA was extracted from biological replicates of each cell line using the RNeasy Mini Kit (74104) (Qiagen). Samples with 0.5–1 ug of RNA and RIN > 7 were used for library preparation and run on NovaSeq S1 flow cell. Read counts were calculated using featureCounts with default parameters, and differential expression analysis was performed on raw counts using edgeR (29, 30). Differentially expressed genes with a p-value < 0.05 were visualized by heatmap. Gene expression data, read counts, and clinical data for TCGA-CESC primary tumors (N=304) were downloaded from NCI Genomic Data Commons (GDC). *PTEN* mutation and copy number status were downloaded from cBioPortal (31).

Stable isotope-based metabolomics

Stable isotope labeling was accomplished using 10 mM uniformly labeled $^{13}C_6$ glucose or 2 mM $^{13}C_5$ glutamine to glucose- or glutamine-free DMEM (Gibco A1443001) supplemented with 10% dialyzed FBS (Cambridge Isotope Laboratories, Tewksbury, MA). Media was supplemented with 2 mM glutamine ($^{13}C_6$ glucose) and 10 mM glucose ($^{13}C_5$ glutamine). Cells were labelled for 18 hours followed by glutamine deprivation or telaglenastat treatment for 48 hours and then processed as described (32). Cells were washed with PBS and LC/MS-grade water, quenched with cold methanol, scraped and transferred to microfuge tubes. Methanol was evaporated using a SpeedVac. Pellets were extracted with 2:2:1 methanol:acetonitrile:water (1 mL per 100 mm plate surface area equivalent). Extracts were reconstituted in 1:2 water:acetonitrile volume normalized to the dry mass of the cell pellet. For media studies, 800 μL of cold methanol:acetonitrile (1:1) was added to 200 μL of media. The solution was vortexed, sonicated, evaporated and re-constituted in 100 μL of acetonitrile:water (2:1). The mixture was then sonicated, centrifuged, and the supernatant was taken for LC/MS analysis. The absolute concentrations of glucose and glutamine were quantified after culturing cells for 48 hours. Known concentrations of $^{13}C_6$ glucose or 2 mM $^{13}C_5$ glutamine were spiked into media samples after extractions. Concentrations were determined by calculating the ratio between the fully unlabeled peak and the fully labelled peak from standards. Consumption rates were normalized to doubling time over the experimental time period. LC/MS analysis was performed by using an Agilent 6540 QTOF interfaced with an Agilent 1290 Infinity II LC system (Agilent Technologies, Santa Clara, CA) equipped with a Sequant ZIC-pHILIC column (100 × 2.1 mm, 5 μm; EMD Millipore, Burlington, MA). Mobile-phase solvents were composed of A=20 mM ammonium acetate and 5 μM ammonium phosphate in water:acetonitrile (95:5) and B=100% acetonitrile. The column was maintained at 40 °C. The following linear gradient was applied at a flow rate of 225 μL/min: 0–1 min: 89.5% B, 1–30 min: 89.5–20% B, 30–33 min: 20% B. The column was re-equilibrated with 20 column volumes of 89.5% B. Injection volumes were 5 μL for all experiments. Data were collected with the following settings: gas, 200 °C at 10 L/min; nebulizer, 44 psi at 2000 V; sheath gas, 300 °C at 12 L/min; capillary, - 3000 V; fragmentor,

175 V; skimmer, 65 V; and scan rate, 1 scan/second; mass range, 60 – 1500 Da. The MS was operated in negative ionization mode for all samples analyzed. MS data were processed with XCMS, X^{13}CMS, and MassHunter Profinder (Agilent Technologies, Santa Clara, CA) (33, 34). The figures and plots were generated using Graphpad Prism.

Glutathione (GSH) and Thioredoxin Reductase (TR) Assay

Cells were grown in 100 mm dishes and treated with or without drugs as described, harvested by scraping and frozen as a dry pellet. Cell pellets were lysed in 50 mM potassium phosphate buffer (pH 7.8) containing 1.34 mM diethylenetriaminepenta-acetic acid, centrifuged at 5000 rpm for 5 minutes and then the supernatant was assayed using a TR kit (Sigma-Aldrich; CS0170). For GSH assay, cells were harvested by scraping using 150 μL of 5% 5-sulfosalicylic acid (Sigma-Aldrich). Total GSH and percent glutathione disulfide (GSSG) content was determined spectrophotometrically by NADPH recycling assay as described (35).

Reactive oxygen species (ROS) quantification

Steady-state levels of reactive oxygen species were estimated using oxidation of the fluorescent dye, 2',7'-dichlorodihydrofluorescein diacetate (H2DCFDA), normalized to the oxidation insensitive analog, 2',7' –dichlorofluorescin diacetate (DCFDA) ,obtained from Molecular Probes (Eugene, OR, U.S.A.). Cells were incubated with H2DCFDA (10 μM) or DCFDA at 37 °C for 30 min in culture media without washing. Samples were analyzed using a flow cytometer (λ_{ex}=495 nm and $\lambda_{emission}$=529 nm band-pass filter). The MFI (mean fluorescence intensity) was analyzed in each sample and corrected for auto-fluorescence from unlabeled cells (36). Mean Florescent Intensity/cell (MFI) results from H2DCFDA labeling were normalized to replicate samples labeled with the oxidation insensitive dye (DCFDA) under each treatment condition.

Western blotting

Western blotting was performed with primary antibodies against phosphorylated and total forms of p70s6k ^{Thr389} and Akt^{Ser473} (1:1000; Cell Signaling Technology, MA), for total forms of PTEN (1:1000; Cell Signaling Technology, MA), GAPDH, Akt (1:1000, Cell Signaling Technology, MA), and for total forms of p70s6k and Actin (1:1000, Santa Cruz Biotechnology, CA) and PC (1:500, Thermo Fisher, MA). Blots were probed with HRP-conjugated anti-rabbit (Cell Signaling Technology, Beverly, MA) or anti-mouse polyclonal IgG secondary antibodies (Santa Cruz Biotechnology, CA) for 1 h at room temperature. For detection, Amersham ECL select (GE-healthcare, PA) was used according to manufacturer's protocol. Images were acquired using Chemidoc Imaging systems (BioRad).

Tumor Growth Delay with and without tumor directed irradiation

All *in vivo* studies were conducted according to the protocols approved by Washington University Division of Comparative Medicine and Institutional Animal Care and Use Committee. For tumor generation, 3.5×10^6 SiHa and or CaSki cells were injected subcutaneously into the left flank of 6–8 week old, female nude mice (Crl:NU(NCr)-Foxn1 nu, Charles River Laboratories, Wilmington, MA) in a half matrigel, half serum-free IMDM

mixture. Initial tumor sizes were recorded using calipers, and mice were grouped (N=5 per treatment group) with 5 mm tumor diameters. For tumor growth delay studies in CaSki tumors, treatment groups included: vehicle, telaglenastat at 50 mg/kg, 100 mg/kg and 200 mg/kg. For telaglenastat treatments, mice were treated three times per week via oral gavage over a period of 37 days. For tumor growth delay studies in SiHa tumors, single fraction radiation doses of 4 Gy were delivered 1 week after initiating treatment with telaglenastat. Targeted radiation delivery was performed using the Xstrahl Small Animal Radiation Research Platform (SARRP) 200 (Xstrahl Life Sciences, Suwannee, GA). Mice were placed on the irradiation platform one at a time and fitted with a nose cone for isofluorane anesthesia. CT images imported into Muriplan were used to select an isocenter. The tumor was then irradiated using anterior-posterior opposed beams using the 10 mm × 10 mm collimator at a dose rate of 3.9 Gy/min. Telaglenastat treatment was continued for 4 weeks after radiation treatment. Tumor measurements were quantified by caliper measurement on a weekly basis for each animal. Statistical comparisons were performed using Restricted Maximum Likelihood (REML) Mixed effect Model with volume as response variable, treatment groups as covariates and replicates and day as random effect.

Results

PI3K-activated cervical cancer cells are sensitive to glutamine deprivation

We determined the sensitivity to glutamine starvation of a panel of cervical cancer cell lines, including those with known PI3K pathway alterations (Figure 1A and Supplementary Table 1). Normalized surviving fractions following glutamine deprivation demonstrated decreased survival in CaSki and C33A cells, while SiHa cells were relatively resistant. To test whether cervical cancer cell dependence on glutamine could be directly influenced by single gene mutations in the PI3K pathway, we generated *PTEN*-deleted cells (SiHa PTEN$^{-/-}$) from parent SiHa cells using CRISPR/Cas9 (Supplementary Figure 1B–C). In contrast to parental SiHa cells, SiHa PTEN$^{-/-}$ cells demonstrated complete attenuation of PTEN and express high levels of phosphorylation of PI3K pathway targets including pAKT (Supplementary Figure 1D). Interestingly, SiHa PTEN$^{-/-}$ cells were more sensitive to glutamine starvation than the parent SiHa cells (Figure 1A), suggesting that *PTEN* deletion and resulting PI3K pathway activation are associated with increased dependency on glutamine metabolism *in vitro*. To demonstrate the prevalence of *PTEN* alterations in human cervical cancer tumors, we analyzed whole transcriptome and exome sequencing data from TCGA cervical cancer (TCGA-CESC) cohort (*N*=304). We observed 35% of primary cervical cancers harbor genomic alterations that decrease *PTEN* expression (Figure 1B–C). To examine the direct effects of *PTEN* loss on gene expression of metabolic pathways, we performed whole transcriptome sequencing of our engineered SiHa cells (Supplementary Tables 2–3). Compared to parental cells, SiHa PTEN$^{-/-}$ cells displayed decreased expression of multiple genes related to glutamine metabolism in addition to several key glycolytic enzymes (Figure 1D–E).

Relative rates of glutamine consumption were compared in cervical cancer cells with and without PI3K pathway mutations. As demonstrated in Figure 2A, CaSki cells consume high levels of glutamine, while SiHa cells consume less. Compared to parental SiHa cells, SiHa

PTEN$^{-/-}$ cells consume higher levels of glutamine and glucose (Figures 2A–B). We compared glucose consumption rates in exhausted media after culturing cells in the presence and absence of glutamine deprivation (Figure 2C). CaSki cells consumed less glucose from the media when glutamine was limiting, while SiHa cells were able to maintain baseline levels of glucose consumption. Compared to parental SiHa cells, SiHa PTEN$^{-/-}$ cells consumed slightly less glucose at baseline but retained the ability to metabolize glucose even in the setting of glutamine deprivation. We performed cell proliferation assays at different time points after the initiation of glutamine starvation (Figure 2D–G). All three *PTEN* mutated or null cell lines (CaSki, C33A and SiHa PTEN$^{-/-}$) displayed significant decreases in cell proliferation after day 4, compared to day 8 in SiHa cells. We compared the relative sensitivity of cervical cancer cell lines to glucose versus glutamine deprivation. Surprisingly, cervical cancer cells were more sensitive to glutamine starvation (Gluc+Gln−) versus glucose (Gluc−Gln+) starvation (Figure 2H–K). When glutamine starvation was combined with glucose starvation (Gluc− Gln−), CaSki cells demonstrated increased dependency on glutamine relative to glucose (Gluc+, Gln−) (Figure 2H), while SiHa cells continued to display intermediate sensitivity to both glucose and glutamine starvation (Figure 2J). Compared to parental SiHa cells, SiHa PTEN$^{-/-}$ cells displayed increased dependency upon glutamine relative to glucose (Figure 2K), suggesting that inhibition of glutamine metabolism may be a more effective metabolic treatment strategy than inhibition of glycolysis in PI3K pathway activated cervical cancers.

Glutamine deprivation induces oxidative stress in glycolytic cervical cancer cells

We determined whether glutamine starvation resulted in decreased availability of glutathione and increased levels of baseline intracellular oxidative stress in cervical cancer cells with and without PI3K pathway activation. As shown in Figure 3A, glutamine deprivation resulted in decreases in total reduced glutathione (GSH) (Figure 3A) with concomitant increases in percent glutathione disulfide (%GSSG), a reliable surrogate measure of intracellular oxidative stress (Figure 3B). Glutamine deprivation was associated with significant increases in intracellular oxidation as evidenced by increases in 2',7'-dichlorodihydrofluorescein diacetate (H2DCFDA) oxidation (Figure 3C) in CaSki cells under conditions of glutamine deprivation, but not in SiHa cells. Consistent with these observations, intracellular NADPH/NADP ratios increased only in CaSki cells as a compensatory mechanism to deal with reactive oxygen species (ROS) accumulation under conditions of glutamine deprivation (Figure 3D). These effects were most pronounced in CaSki versus SiHa cells, an effect related to increased reducing capacity via alternative pathways such as thioredoxin in SiHa cells (Figure 3E). As previously reported by our group (21), upregulation of thioredoxin reductase (*TXNRD*) is an alternative mechanism used in some cervical cancer cells to maintain redox balance, an observation that becomes clinically relevant when selecting drug strategies designed to increase oxidative stress. Importantly, overexpression of *TXNRD* and other genes within this pathway is not a cancer cell line specific phenomenon, but rather a relevant potential treatment resistance mechanism observed in human cervical as well as other cancers. As shown in Supplementary Figure 2 A–C, we have identified overexpression of *TXNRD* and related transcripts within TCGA cervical cancer data set (37–39). Oxidative stress parameters were similar in SiHa cells with and without *PTEN* deletion, suggesting that PI3K pathway signaling is less relevant to the

maintenance of redox balance when *TXNRD* is overexpressed. These results demonstrate that glutamine deprivation is associated with increased baseline oxidative stress in cervical cancer cells, but the extent of this particular effect is maximized in highly glycolytic cervical cancer cells that rely on the glutathione system to maintain redox balance (i.e., CaSki cells). Increases in intracellular oxidative stress induced by glutamine deprivation may be limited by increased expression of redox metabolic pathways other than glutathione (i.e., thioredoxin reductase in SiHa cells and some human cervical tumors).

Inhibition of glutaminase is selectively cytotoxic for PI3K activated cervical cancer cells via increases in intracellular oxidative stress

We next wanted to determine whether inhibition of glutaminase with telaglenastat would be selectively cytotoxic for glutamine-dependent cervical cancers and determine to what extent this sensitivity was dependent upon mutations in the PI3K pathway. To begin, we modeled dose-response curves by performing cell viability assays for telaglenastat monotherapy in a panel of cervical cancer cell lines including CaSki, SiHa, and SiHa PTEN$^{-/-}$ cell lines (Figure 4A). In general, sensitivity to telaglenastat monotherapy was more pronounced in cervical cancer cell lines with PI3K pathway mutations compared to those without, including HPV negative lines HT-3 and C-41, with the exception of C33A cells which demonstrated intermediate sensitivity (Figure 4A and Supplemental Figure 2D). Interestingly, sensitivity to telaglenastat monotherapy was most pronounced in CaSki and SiHa PTEN$^{-/-}$ cells relative to parent SiHa cells, even though there was relatively little difference in oxidative stress parameters under conditions of glutamine deprivation in SiHa versus SiHa PTEN$^{-/-}$ cells, suggesting that metabolic outputs from glutamine other than glutathione may contribute to telaglenastat sensitivity (Figures 3 and 4A). Quantification of total GSH, %GSSG and TR activity before and after telaglenastat treatment confirmed increases in oxidative stress with associated decreases in the reducing capacity through glutathione after telaglenastat treatment in all cell lines tested (Figure 4B–D). Importantly, the cytotoxic effects of telaglenastat could be rescued by the addition of the thiol antioxidant, N-acetylcysteine (NAC) (Figure 4E–F) confirming that the mechanism of action of telaglenastat includes treatment related increases in thiol-dependent oxidative stress.

The efficacy of telaglenastat monotherapy in glutamine dependent cervical cancer tumors *in vivo* was tested using CaSki tumor implants grown in the flanks of immune compromised mice (Figures 4G–H and Supplementary Figure 8A–C). Treatment with telaglenastat monotherapy at 200 mg/kg in this model resulted in tumor regression with no observable toxicities and no evidence of tumor regrowth after 37 days (Supplementary Figure 8B). These experiments were repeated with telaglenastat dose de-escalation, with telaglenastat administered at 50 and 100 mg/kg every other day. Importantly, telaglenastat using this dose schedule, which includes significantly lower doses and less frequent administration than has been used in previous preclinical studies with other tumor models, resulted in tumor regression, suggesting that telaglenastat monotherapy (50 mg/kg) is highly potent and effective in appropriately selected glutamine-dependent cervical tumor models (Figure 4G). SiHa xenograft tumor regression was observed with telaglenastat monotherapy at a concentration of 100 mg/kg after day 15. (Figure 4H).

Stable isotope labeling demonstrates targetable outputs of glutamine metabolism in addition to glutathione in cervical cancer cells

To determine all the metabolic contributions of glutamine in cervical cancer cells with and without PI3K pathway activation, we performed isotope-tracing studies with uniformly labeled ^{13}C glutamine in CaSki, SiHa and SiHa PTEN$^{-/-}$ cells. As shown in Figures 5A–B and Supplementary Figure 3, cervical cancer cells generated glutamate and the tricarboxylic acid (TCA) cycle intermediate α-ketoglutarate from exogenous glutamine as evidenced by incorporation of labeled carbon into the m+5 fraction of each metabolite. The generation of labeled glutamate and α-ketoglutarate from exogenous $^{13}C_5$ glutamine was increased in CaSki cells relative to SiHa cells, and in SiHa PTEN$^{-/-}$ cells relative to parental SiHa cells, suggesting that PI3K pathway activation facilitates this process. As expected, cervical cancer cells also generated glutathione (GSH) from exogenous glutamine, as evidenced by the incorporation of labeled carbon from $^{13}C_5$ glutamine into the m + 5 fraction of GSH (Figure 5C). Similar to the effects on TCA cycle intermediates, the generation of labeled glutathione from exogenous $^{13}C_5$ glutamine was increased in CaSki cells relative to SiHa cells, and in SiHa PTEN$^{-/-}$ cells relative to parental SiHa cells, suggesting that PI3K pathway activation facilitates this process.

In our previous experiments, we demonstrated that glutamine deprivation results in increased oxidative stress in cervical cancer cells via decreases in the availability of glutathione, an effect which is most prominent in cervical cancer cell lines such as CaSki that do not upregulate alternative pathways for maintaining redox balance (Figure 3). To examine the effects of glutamine deprivation on the metabolic fates of glucose, we performed LC/MS-based isotope-tracer studies with uniformly labeled glucose ($^{13}C_6$ glucose) performed in the presence and absence of glutamine deprivation (Figures 5E–H and Supplementary Figures 4–7). Glutamine deprivation resulted in increased glucose carbon utilization through TCA cycle via pyruvate anaplerosis. This was evidenced by increased labeling of malate (Figure 5E) and citrate (Figure 5F) (m+ 3) fractions in all three cell lines from ^{13}C-glucose under conditions of glutamine starvation. Interestingly, SiHa cells displayed an increased capacity to divert glucose carbon into the TCA cycle via pyruvate anaplerosis as evidenced by higher m+3 fractions (Figure 5E–F), an effect that was associated with increased expression of pyruvate carboxylase and successful rescue of clonogenic survival with the addition of pyruvate or α-ketoglutarate in SiHa cells (Supplementary Figures 6–7). Glucose flux to the pentose phosphate pathway (PPP) was also affected by glutamine starvation, as demonstrated by decreased ribose labeling in ADP (m+5) in CaSki (Figure 5G) and SiHa cells under conditions of glutamine starvation. Consistent with this observation, we also saw decreases in the concentrations of purine nucleotides with glutamine deprivation (Figure 5H). These results suggest that inhibition of glutamine metabolism could be combined with other strategies in addition to those that target redox balance, such as drugs that target mitochondrial metabolism or DNA synthesis and repair, as means to achieve therapeutic synergy.

Pharmacologic inhibition of glutaminase can be combined with radiation to enhance treatment efficacy

To determine whether telaglenastat monotherapy was sufficient to eliminate reducing capacity via glutathione, we performed clonogenic cell survival assays in CaSki, SiHa and SiHa PTEN$^{-/-}$ cells with telaglenastat or telaglenastat combined with L-buthionine sulfoximine (BSO), an inhibitor of the rate limiting step of glutathione synthesis. As we previously identified upregulation of redox metabolic pathways other than glutathione (TR) in SiHa cells, we also included Auranofin (AUR), an inhibitor of thioredoxin reductase (TR) in these experiments. As shown in (Figure 6A–C), treatment with telaglenastat alone reduced cell survival in CaSki and SiHa PTEN$^{-/-}$ cells, but not in SiHa parental cells, an effect that may be due to increased capacity for maintaining redox balance via the thioredoxin system in this cell line (Figure 3E and Figure 4D). The addition of BSO increased telaglenastat cytotoxicity in all three cell lines, with relatively little additional benefit derived from the addition of AUR, even in SiHa parental cells. Interestingly, telaglenastat and AUR was more effective than telaglenastat alone in CaSki and SiHa PTEN $^{-/-}$, but not in SiHa parental cells, an effect that may be related to treatment induced TR upregulation.

The primary treatment strategy for locally advanced cervical cancer is pelvic radiation, a treatment which is also known to increase tumor cell oxidative stress. In order to determine whether telaglenastat could serve as a radiation modifier *in vitro*, we performed clonogenic cell survival assays with increasing single fraction doses of RT in the presence and absence of telaglenastat in CaSki, SiHa and SiHa PTEN−/− cells (Figure 6D–F). These results demonstrate that telaglenastat enhances the effect of RT with a Dose Modifying Factor (DMF) of 1.9, 1.2 and 1.7 in CaSki, SiHa and SiHa PTEN−/− cells, respectively. The radiation response of the corresponding normal cervical epithelial cell HCvEpC line was not modified by telaglenastat at any of the doses tested (Figure 6G). Finally, in an *in vivo* experiment with SiHa xenograft tumors in immune compromised mice, we observed increased tumor control in response to tumor directed radiation when administered with concurrent telaglenastat, suggesting that telaglenastat can function as an radiation modifier *in vivo* (Figure 6H and Supplementary Figure 8 D–E).

Discussion

The purpose of the current study was to test whether radiation resistant cervical cancers are dependent upon glutamine metabolism, and to determine whether metabolic reprogramming driven by PI3K pathway mutations predicts sensitivity of cervical cancer to telaglenastat. Using a combination of *in vitro* and *in vivo* model systems, including *PTEN*-deleted cells (SiHa PTEN$^{-/}$) that we engineered from parent SiHa cells using CRISPR/Cas9 technology, we demonstrate that *PTEN* is frequently altered in human cervix tumors, preclinical models of PI3K activated tumors are uniquely sensitive to glutamine deprivation (Figures 1 and 2), and that glutamine deprivation and treatment with telaglenastat results in increases in intracellular oxidative stress in models of treatment refractory cervical cancer (Figure 3 and 4). PTEN is a regulator of glutamine metabolism, and our results confirm that *PTEN* loss leads to increased dependency on glutamine with resultant increased sensitivity to

telaglenastat in cervix cancer (40). Importantly, we show that inhibition of glutaminase is selectively cytotoxic for PI3K activated cervical cancers, and that this effect is due to resultant decreases in intracellular reducing capacity derived from glutathione (GSH) (Figure 4 and Figure 6I). As such, telaglenastat is particularly potent and effective even as monotherapy in appropriately selected glutamine-dependent PI3K activated cervical cancer models (Figure 4G). It is important to note that while GSH levels are decreased, they are not completely eliminated by telaglenastat treatment in our models, allowing for synergistic activity with other agents, such as BSO, that target the glutathione system (Figure 6A–C).

Our results support published data that link telaglenastat efficacy to increased oxidative stress in other cancers. Biancur *et al* reported the accumulation of reactive oxygen species in response to telaglenastat treatment and synergistic response with BSO in pancreatic ductal adenocarcinoma (PDAC) (41). Similarly, telaglenastat combined with β-lapachone results in oxidative imbalance and DNA damage-induced cell death in *KRAS* mutant/*NQO1* over-expressing PDAC models (42). In contrast to pancreatic and lung cancers, *KRAS*, *LKB1* and *NRF2/KEAP1* are not frequently mutated in human cervix cancer (43–45) (12). Our results demonstrate for the first time that mutations in the PI3K pathway play a critical role in maintaining redox homeostasis and glutamine dependency in cervical cancer, and suggest that activation of the PI3K pathway by *PTEN* alterations could be used as a biomarker to predict sensitivity to telaglenastat. These results are consistent with existing evidence for increased telaglenastat sensitivity observed in preclinical models of *PIK3CA* mutated colon cancer (46, 47).

To further increase the translational relevance of our findings, we have combined telaglenastat with radiation treatment, the standard of care for locally advanced cervical cancer, and shown that telaglenastat can be used as a radiation modifier both *in vitro* and *in vivo* (Figure 6D–F). Previous reports suggested telaglenastat enhanced radiation sensitivity in lung cancer cells and glutamine dependent, *IDH1*-mutant glioma cells (48, 49). An ongoing phase 1b clinical trial in patients with *IDH*-mutated diffuse or anaplastic astrocytoma is determining the best dose of telaglenastat in combination with radiotherapy and temozolomide (50). Our results support investigating telaglenastat in combination with definitive radiation in cervical cancer in the context of clinical trials. Importantly, although we show that the radiation modifying effect of telaglenastat is likely due to increased thiol-mediated oxidative stress in cervical cancer, telaglenastat has other metabolic effects that may contribute to radiation sensitivity. Using stable isotope labeling, we show that cervical cancer cells use glutamine not only for maintaining glutathione levels, but also for replenishing TCA cycle intermediates needed for energy balance (Figure 5A–D) and using ^{13}C labeled glucose, we demonstrate that some cervical cancer cell lines have increased capacity for pyruvate anaplerosis (Figure 5E–F and Figure 6I), but all cell lines demonstrate decreased nucleotide production in the setting of glutamine deprivation. These results suggest that, in addition to increasing oxidative stress, telaglenastat also has the capacity to limit DNA repair via decreased nucleotide production, which supports the rationale combination of telaglenastat with a variety of DNA damaging agents and drugs that induce redox stress. Work is ongoing in our lab to determine to what extent the radiation modifying properties of telaglenastat are dependent upon decreased capacity for DNA repair, and to

optimize drug combination schedules with standard of care chemotherapies including cisplatin.

In summary, we report for the first-time preclinical data to support the use of telaglenastat for radiation resistant cervical cancers, and demonstrate that PI3K pathway mutations including *PTEN* alterations may be used as a predictive biomarker for telaglenastat sensitivity. Here, we show that cervix cancer patients with PI3K pathway mutant, glutamine dependent tumors could potentially benefit from telaglenastat and the rationale combination of telaglenastat with radiation and BSO with or without AUR. Given that telaglenastat (registrational phase 2 clinical trial drug), BSO and AUR are FDA approved drugs, if additional experiments in other xenograft models of cervical cancer confirm our findings, then they can be translated into clinical trials for patients with PI3K activated cervical cancer.

Supplementary Material

Refer to Web version on PubMed Central for supplementary material.

Acknowledgements

We would like to thank Cedric Mpoy for technical assistance.

Financial support:

This work was supported by NIH R01CA181745 to JKS; R35ES028365 to GJP; Radiation and Free Radical Research Core P30CA086862 and P01CA217797 to DRS and MLM.

References

1. Arbyn MWE, Bruni L, De Sanjose S, Saraiya M, Ferlay J, Bray F. Estimates of incidence and mortality of cervical cancer in 2018: a worldwide analysis. The Lancet. 2019;8(2):PE191–E203.
2. Rodin D, Burger EA, Atun R, Barton M, Gospodarowicz M, Grover S, et al. Scale-up of radiotherapy for cervical cancer in the era of human papillomavirus vaccination in low-income and middle-income countries: a model-based analysis of need and economic impact. Lancet Oncol. 2019.
3. Morris M, Eifel PJ, Lu J, Grigsby PW, Levenback C, Stevens RE, et al. Pelvic radiation with concurrent chemotherapy compared with pelvic and para-aortic radiation for high-risk cervical cancer. N Engl J Med. 1999;340(15):1137–43. [PubMed: 10202164]
4. Eifel PJ, Winter K, Morris M, Levenback C, Grigsby PW, Cooper J, et al. Pelvic irradiation with concurrent chemotherapy versus pelvic and para-aortic irradiation for high-risk cervical cancer: an update of radiation therapy oncology group trial (RTOG) 90–01. J Clin Oncol. 2004;22(5):872–80. [PubMed: 14990643]
5. Hockel M, Dornhofer N. Pelvic exenteration for gynaecological tumours: achievements and unanswered questions. Lancet Oncol. 2006;7(10):837–47. [PubMed: 17012046]
6. Tewari KS, Sill MW, Penson RT, Huang H, Ramondetta LM, Landrum LM, et al. Bevacizumab for advanced cervical cancer: final overall survival and adverse event analysis of a randomised, controlled, open-label, phase 3 trial (Gynecologic Oncology Group 240). Lancet. 2017;390(10103):1654–63. [PubMed: 28756902]
7. Penson RT, Huang HQ, Wenzel LB, Monk BJ, Stockman S, Long HJ 3rd, et al. Bevacizumab for advanced cervical cancer: patient-reported outcomes of a randomised, phase 3 trial (NRG Oncology-Gynecologic Oncology Group protocol 240). Lancet Oncol. 2015;16(3):301–11. [PubMed: 25638326]

8. Song S, Pitot HC, Lambert PF. The human papillomavirus type 16 E6 gene alone is sufficient to induce carcinomas in transgenic animals. J Virol. 1999;73(7):5887–93. [PubMed: 10364340]
9. Brake T, Connor JP, Petereit DG, Lambert PF. Comparative analysis of cervical cancer in women and in a human papillomavirus-transgenic mouse model: identification of minichromosome maintenance protein 7 as an informative biomarker for human cervical cancer. Cancer Res. 2003;63(23):8173–80. [PubMed: 14678972]
10. Brake T, Lambert PF. Estrogen contributes to the onset, persistence, and malignant progression of cervical cancer in a human papillomavirus-transgenic mouse model. Proc Natl Acad Sci U S A. 2005;102(7):2490–5. [PubMed: 15699322]
11. Rashmi R, DeSelm C, Helms C, Bowcock A, Rogers BE, Rader JL, et al. AKT inhibitors promote cell death in cervical cancer through disruption of mTOR signaling and glucose uptake. PLoS One. 2014;9(4):e92948. [PubMed: 24705275]
12. Ojesina AI, Lichtenstein L, Freeman SS, Pedamallu CS, Imaz-Rosshandler I, Pugh TJ, et al. Landscape of genomic alterations in cervical carcinomas. Nature. 2014;506(7488):371–5. [PubMed: 24390348]
13. Cancer Genome Atlas Research N, Albert Einstein College of M, Analytical Biological S, Barretos Cancer H, Baylor College of M, Beckman Research Institute of City of H, et al. Integrated genomic and molecular characterization of cervical cancer. Nature. 2017;543(7645):378–84. [PubMed: 28112728]
14. de la Rochefordiere A, Kamal M, Floquet A, Thomas L, Petrow P, Petit T, et al. PIK3CA Pathway Mutations Predictive of Poor Response Following Standard Radiochemotherapy +/− Cetuximab in Cervical Cancer Patients. Clin Cancer Res. 2015;21(11):2530–7. [PubMed: 25724520]
15. Arjumand W, Merry CD, Wang C, Saba E, McIntyre JB, Fang S, et al. Phosphatidyl inositol-3 kinase (PIK3CA) E545K mutation confers cisplatin resistance and a migratory phenotype in cervical cancer cells. Oncotarget. 2016;7(50):82424–39. [PubMed: 27489350]
16. Grigsby P, Elhammali A, Ruiz F, Markovina S, McLellan MD, Miller CA, et al. Clinical outcomes and differential effects of PI3K pathway mutation in obese versus non-obese patients with cervical cancer. Oncotarget. 2018;9(3):4061–73. [PubMed: 29423104]
17. Xue F, Lin LL, Dehdashti F, Miller TR, Siegel BA, Grigsby PW. F-18 fluorodeoxyglucose uptake in primary cervical cancer as an indicator of prognosis after radiation therapy. Gynecol Oncol. 2006;101(1):147–51. [PubMed: 16263155]
18. Kidd EA, Siegel BA, Dehdashti F, Grigsby PW. The standardized uptake value for F-18 fluorodeoxyglucose is a sensitive predictive biomarker for cervical cancer treatment response and survival. Cancer. 2007;110(8):1738–44. [PubMed: 17786947]
19. Busk M, Horsman MR, Kristjansen PE, van der Kogel AJ, Bussink J, Overgaard J. Aerobic glycolysis in cancers: implications for the usability of oxygen-responsive genes and fluorodeoxyglucose-PET as markers of tissue hypoxia. Int J Cancer. 2008;122(12):2726–34. [PubMed: 18351643]
20. Onal C, Reyhan M, Parlak C, Guler OC, Oymak E. Prognostic value of pretreatment 18F-fluorodeoxyglucose uptake in patients with cervical cancer treated with definitive chemoradiotherapy. Int J Gynecol Cancer. 2013;23(6):1104–10. [PubMed: 23792605]
21. Rashmi R, Huang X, Floberg JM, Elhammali AE, McCormick ML, Patti GJ, et al. Radioresistant Cervical Cancers Are Sensitive to Inhibition of Glycolysis and Redox Metabolism. Cancer Res. 2018;78(6):1392–403. [PubMed: 29339540]
22. Altman BJ, Stine ZE, Dang CV. From Krebs to clinic: glutamine metabolism to cancer therapy. Nat Rev Cancer. 2016;16(10):619–34. [PubMed: 27492215]
23. Momcilovic M, Bailey ST, Lee JT, Fishbein MC, Braas D, Go J, et al. The GSK3 Signaling Axis Regulates Adaptive Glutamine Metabolism in Lung Squamous Cell Carcinoma. Cancer Cell. 2018;33(5):905–21 e5. [PubMed: 29763624]
24. Abu Aboud O, Habib SL, Trott J, Stewart B, Liang S, Chaudhari AJ, et al. Glutamine Addiction in Kidney Cancer Suppresses Oxidative Stress and Can Be Exploited for Real-Time Imaging. Cancer Res. 2017;77(23):6746–58. [PubMed: 29021138]

25. Jones AT, Narov K, Yang J, Sampson JR, Shen MH. Efficacy of Dual Inhibition of Glycolysis and Glutaminolysis for Therapy of Renal Lesions in Tsc2(+/−) Mice. Neoplasia 2019;21(2):230–8. [PubMed: 30622053]
26. Song M, Kim SH, Im CY, Hwang HJ. Recent Development of Small Molecule Glutaminase Inhibitors. Curr Top Med Chem. 2018;18(6):432–43. [PubMed: 29793408]
27. Gross MI, Demo SD, Dennison JB, Chen L, Chernov-Rogan T, Goyal B, et al. Antitumor activity of the glutaminase inhibitor CB-839 in triple-negative breast cancer. Mol Cancer Ther. 2014;13(4):890–901. [PubMed: 24523301]
28. Bell CC, Magor GW, Gillinder KR, Perkins AC. A high-throughput screening strategy for detecting CRISPR-Cas9 induced mutations using next-generation sequencing. BMC Genomics. 2014;15:1002. [PubMed: 25409780]
29. Aleshkin VA, Vashakmadze LA, Aleshkina TN, Stenina OI. [Acute-phase proteins in the diagnosis of the extent of the pathological process in stomach cancer]. Sov Med. 1986(2):25–9.
30. Robinson MD, McCarthy DJ, Smyth GK. edgeR: a Bioconductor package for differential expression analysis of digital gene expression data. Bioinformatics. 2010;26(1):139–40. [PubMed: 19910308]
31. Gao J, Aksoy BA, Dogrusoz U, Dresdner G, Gross B, Sumer SO, et al. Integrative analysis of complex cancer genomics and clinical profiles using the cBioPortal. Sci Signal. 2013;6(269):pl1.
32. Spalding JL, Naser FJ, Mahieu NG, Johnson SL, Patti GJ. Trace Phosphate Improves ZIC-pHILIC Peak Shape, Sensitivity, and Coverage for Untargeted Metabolomics. J Proteome Res. 2018;17(10):3537–46. [PubMed: 30160483]
33. Smith CA, Want EJ, O'Maille G, Abagyan R, Siuzdak G. XCMS: processing mass spectrometry data for metabolite profiling using nonlinear peak alignment, matching, and identification. Anal Chem. 2006;78(3):779–87. [PubMed: 16448051]
34. Huang X, Chen YJ, Cho K, Nikolskiy I, Crawford PA, Patti GJ. X13CMS: global tracking of isotopic labels in untargeted metabolomics. Anal Chem. 2014;86(3):1632–9. [PubMed: 24397582]
35. Fath MA, Ahmad IM, Smith CJ, Spence J, Spitz DR. Enhancement of carboplatin-mediated lung cancer cell killing by simultaneous disruption of glutathione and thioredoxin metabolism. Clin Cancer Res. 2011;17(19):6206–17. [PubMed: 21844013]
36. Aykin-Burns N, Ahmad IM, Zhu Y, Oberley LW, Spitz DR. Increased levels of superoxide and H2O2 mediate the differential susceptibility of cancer cells versus normal cells to glucose deprivation. Biochem J. 2009;418(1):29–37. [PubMed: 18937644]
37. Esen H, Feyzioglu B, Erdi F, Keskin F, Kaya B, Demir LS. High thioredoxin reductase 1 expression in meningiomas undergoing malignant progression. Brain Tumor Pathol. 2015;32(3):195–201. [PubMed: 25592259]
38. Lincoln DT, Al-Yatama F, Mohammed FM, Al-Banaw AG, Al-Bader M, Burge M, et al. Thioredoxin and thioredoxin reductase expression in thyroid cancer depends on tumour aggressiveness. Anticancer Res. 2010;30(3):767–75. [PubMed: 20392995]
39. Yan X, Zhang X, Wang L, Zhang R, Pu X, Wu S, et al. Inhibition of Thioredoxin/Thioredoxin Reductase Induces Synthetic Lethality in Lung Cancers with Compromised Glutathione Homeostasis. Cancer Res. 2019;79(1):125–32. [PubMed: 30401714]
40. Garcia-Cao I, Song MS, Hobbs RM, Laurent G, Giorgi C, de Boer VC, et al. Systemic elevation of PTEN induces a tumor-suppressive metabolic state. Cell. 2012;149(1):49–62. [PubMed: 22401813]
41. Biancur DE, Paulo JA, Malachowska B, Quiles Del Rey M, Sousa CM, Wang X, et al. Compensatory metabolic networks in pancreatic cancers upon perturbation of glutamine metabolism. Nat Commun. 2017;8:15965. [PubMed: 28671190]
42. Chakrabarti G, Moore ZR, Luo X, Ilcheva M, Ali A, Padanad M, et al. Targeting glutamine metabolism sensitizes pancreatic cancer to PARP-driven metabolic catastrophe induced by ss-lapachone. Cancer Metab. 2015;3:12. [PubMed: 26462257]
43. Koppula P, Zhang Y, Shi J, Li W, Gan B. The glutamate/cystine antiporter SLC7A11/xCT enhances cancer cell dependency on glucose by exporting glutamate. J Biol Chem. 2017;292(34):14240–9. [PubMed: 28630042]

44. Romero R, Sayin VI, Davidson SM, Bauer MR, Singh SX, LeBoeuf SE, et al. Keap1 loss promotes Kras-driven lung cancer and results in dependence on glutaminolysis. Nat Med. 2017;23(11):1362–8. [PubMed: 28967920]

45. Shin CS, Mishra P, Watrous JD, Carelli V, D'Aurelio M, Jain M, et al. The glutamate/cystine xCT antiporter antagonizes glutamine metabolism and reduces nutrient flexibility. Nat Commun. 2017;8:15074. [PubMed: 28429737]

46. Hao Y, Samuels Y, Li Q, Krokowski D, Guan B-J, Wang C, et al. Oncogenic PIK3CA mutations reprogram glutamine metabolism in colorectal cancer. Nature Communications. 2016;7(1):11971.

47. Zhao Y, Zhao X, Chen V, Feng Y, Wang L, Croniger C, et al. Colorectal cancers utilize glutamine as an anaplerotic substrate of the TCA cycle in vivo. Scientific Reports. 2019;9(1):19180. [PubMed: 31844152]

48. Boysen G, Jamshidi-Parsian A, Davis MA, Siegel ER, Simecka CM, Kore RA, et al. Glutaminase inhibitor CB-839 increases radiation sensitivity of lung tumor cells and human lung tumor xenografts in mice. Int J Radiat Biol. 2019;95(4):436–42. [PubMed: 30557074]

49. McBrayer SK, Mayers JR, DiNatale GJ, Shi DD, Khanal J, Chakraborty AA, et al. Transaminase Inhibition by 2-Hydroxyglutarate Impairs Glutamate Biosynthesis and Redox Homeostasis in Glioma. Cell. 2018;175(1):101–16 e25. [PubMed: 30220459]

50. CB-839 With Radiation Therapy and Temozolomide in Treating Participants With IDH-Mutated Diffuse Astrocytoma or Anaplastic Astrocytoma [Available from: https://ClinicalTrials.gov/show/NCT03528642.

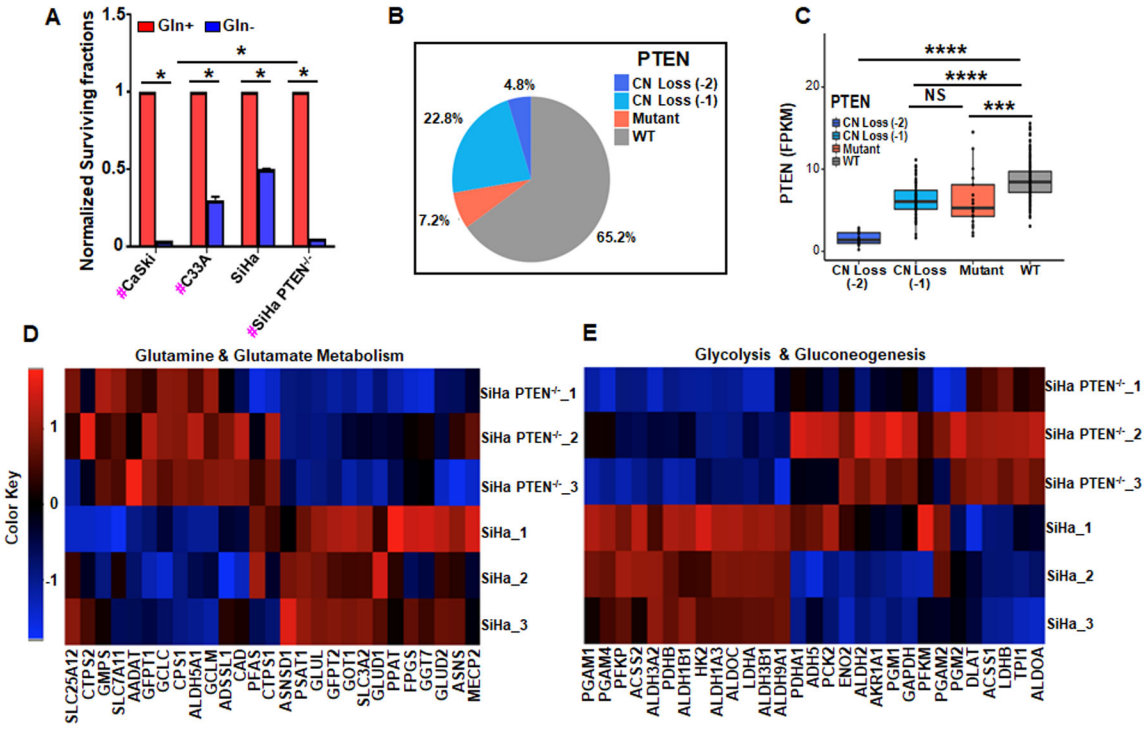

Figure 1. PTEN is frequently altered in cervical cancer, associated with sensitivity to glutamine starvation and regulation of metabolic genes.

(A). Clonogenic cell survival assays for CaSki, C33A, SiHa, and SiHa PTEN$^{-/-}$ in buffered media with and without glutamine (Gln+ and Gln−). Cells were grown in glutamine and pyruvate-free media (CaSki-5 days and C33A, SiHa and SiHa PTEN$^{-/-}$ - 10 days) and plated for clonogenic cell survival assay in media supplemented with 2 mM glutamine. Cell lines with PI3K pathway mutation are marked by #. **(B).** TCGA primary cervical cancer (TCGA-CESC) samples with *PTEN*-inactivating alterations, including 4.8% with deep copy number loss (−2), 22.8% with shallow copy number loss (−1), and ~7.2% with single-nucleotide variants (mut). "−2" (or deep deletion) indicates a deep loss, possibly a homozygous deletion, and "−1" (or shallow deletion) indicates a shallow loss, possibly a heterozygous deletion. **(C).** *PTEN* alterations significantly down-regulate *PTEN* gene expression (FPKM) in cervix tumor samples from the TCGA-CESC cohort. Samples with mutations and shallow deletions show lower *PTEN* expression compared to samples with wild type (WT) *PTEN*. Samples with deep deletions show the lowest *PTEN* expression levels. **(D).** Changes in glutamine and glutamate metabolism related gene expression after *PTEN* loss in SiHa cell lines. SiHa_1, SiHa_2, and SiHa_3 (biological replicates of SiHa) cells have wild-type *PTEN*, while PTEN$^{-/-}$_1, PTEN$^{-/-}$_2, and PTEN$^{-/-}$_3 (biological replicates of SiHa PTEN$^{-/-}$) cells are derived through knocking out *PTEN* in SiHa cells (See Methods and Supplementary Figure 1). **(E).** Changes in glycolysis and gluconeogenesis related gene expression after *PTEN* loss in SiHa cell lines.

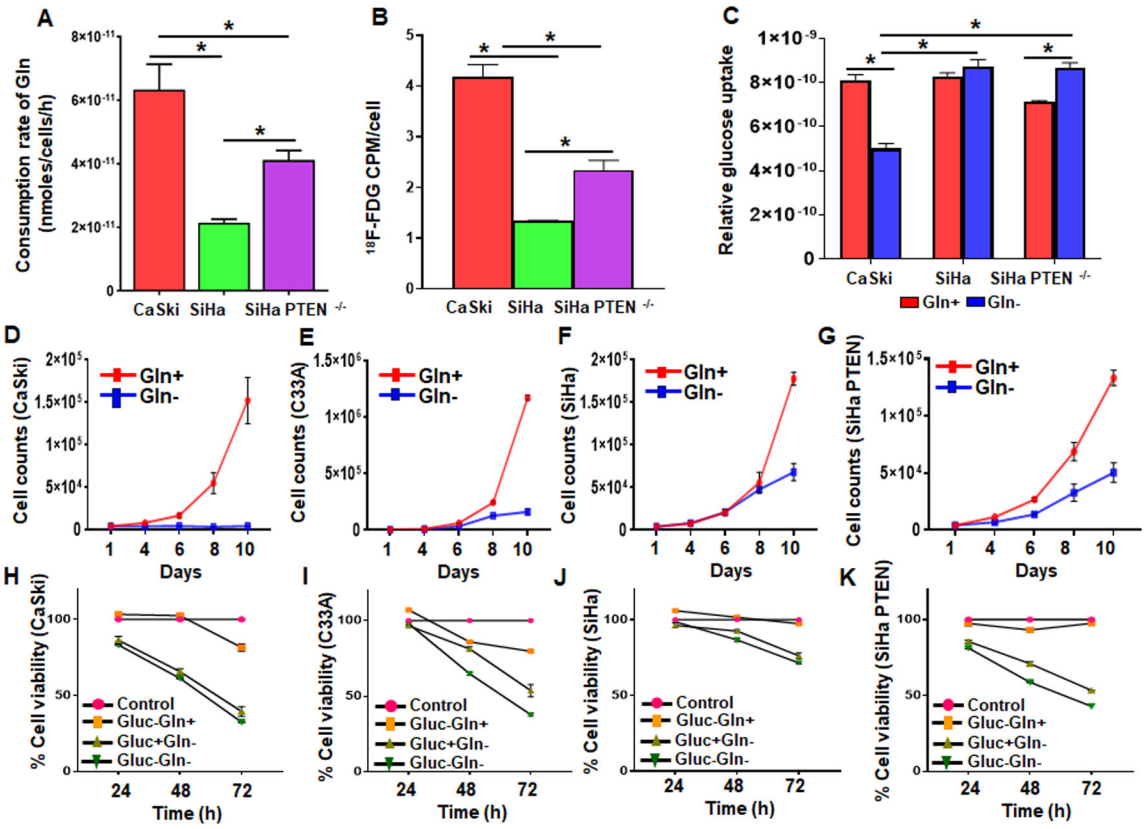

Figure 2. PI3K activated cervical cancer cells are sensitive to Glutamine deprivation.

(**A**) Consumption rate of Glutamine (Gln) (nmol/cell/h) for CaSki, SiHa and SiHa PTEN$^{-/-}$ cells in media with $^{13}C_5$ labeled Gln. Results are normalized to glucose uptake. (**B**) Glucose uptake quantified by ^{18}F-Fluoro-deoxy-glucose (FDG) uptake for CaSki, SiHa and SiHa PTEN$^{-/-}$ cells. (**C**) Glucose consumption from media for cells cultured in the presence and absence of glutamine starvation. (**D-G**) Cell proliferation assays for CaSki, C33A, SiHa and SiHa PTEN$^{-/-}$ cells in media with and without (Gln+ and Gln−) glutamine. Cells were seeded in 12 well plate at the density of 4000 cells per well. Relative cell density is plotted in Y axis with time as a function in X-axis. (**H-K**) Cell viability assays for CaSki, C33A, SiHa and SiHa PTEN$^{-/-}$ cells in media with (Gluc+) and without glucose (Gluc−) and or glutamine (Gln+ and Gln−). *Statistical analysis:* Error bars represent ± SD of N=3 experiments performed on different days. Two tailed paired student's test was performed and asterisks represents * p <0.05.

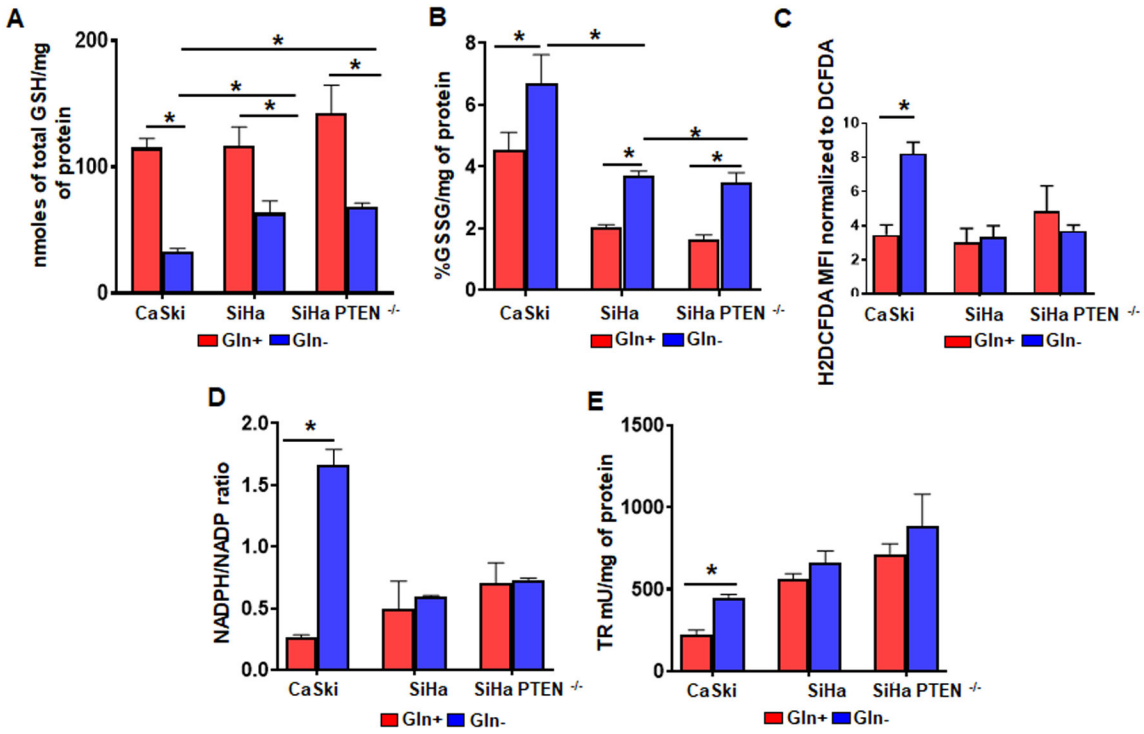

Figure 3. Glutamine deprivation induces oxidative stress in cervical cancer cells

(A-B). Total Glutathione (GSH) level (moles of GSH/mg of protein) and percent GSSG (% of total cellular GSH present in the form of GSSG) for CaSki, SiHa and SiHa PTEN$^{-/-}$ cells grown with (Gln+) and without (Gln−) glutamine for 48 hrs. **(C).** Reactive oxygen species (ROS) quantified by 2',7'-dichlorodihydrofluorescein diacetate (H2DCFDA) oxidation in CaSki, SiHa and SiHa PTEN$^{-/-}$ cells with (Gln+) and without (Gln−) glutamine. **(D).** NADPH/NADP ratio for CaSki, SiHa and SiHa PTEN$^{-/-}$ cells grown with (Gln+) and without (Gln−) glutamine. **(E).** Thioredoxin reductase (TR) activity (mU/mg of protein) for CaSki, SiHa and SiHa PTEN$^{-/-}$ cells grown with (Gln+) and without (Gln−) glutamine for 48 hrs. *Statistical analysis:* Error bars represent ± SD of N=3 experiments performed on different days. Two tailed paired student's test was performed and asterisks represents * $p < 0.05$.

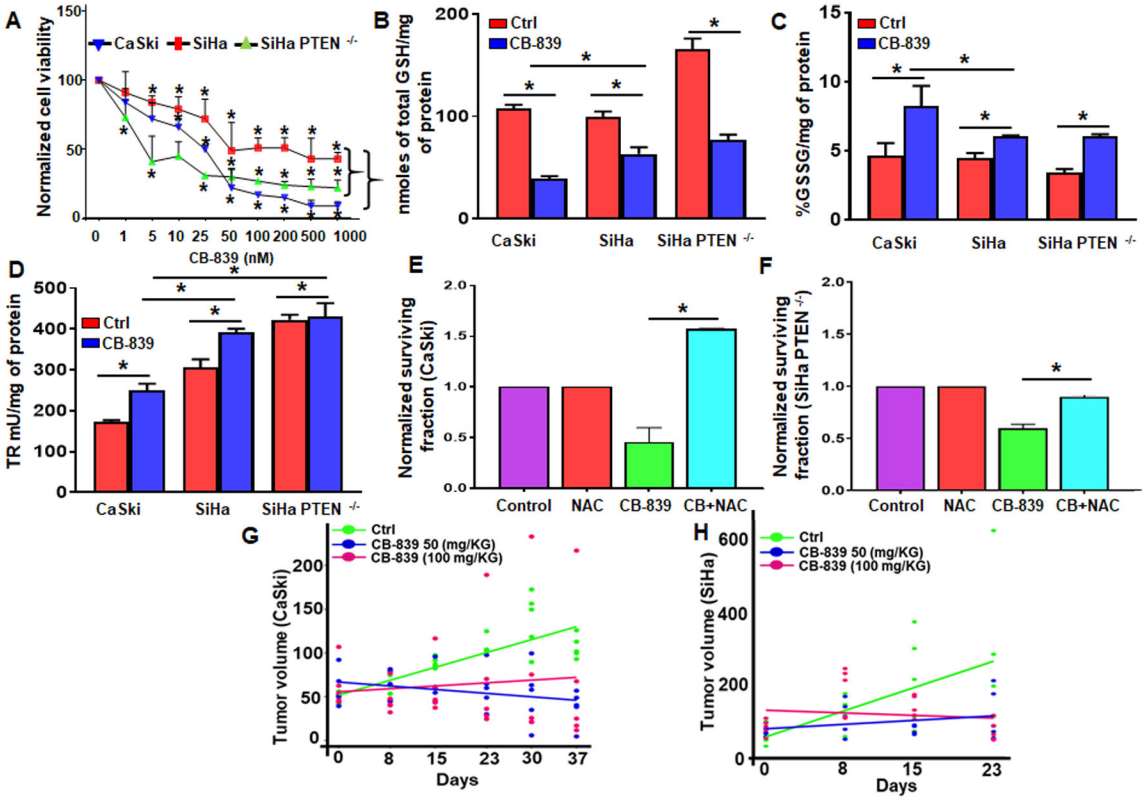

Figure 4. Inhibition of glutaminase is selectively cytotoxic for glycolytic PI3K activated cervical cancer cells via increases in intracellular oxidative stress.

(A) Dose response curve for telaglenastat monotherapy in CaSki, SiHa and SiHa PTEN$^{-/-}$ cells. **(B-D).** Telaglenastat alteration of intracellular redox pools were measured by quantifying levels of reduced glutathione (GSH), percent oxidized glutathione (%GSSG) and thioredoxin reductase (TR) activity after treating cells with 50 nM of telaglenastat for 48hr. **(E-F).** Cytotoxic effects of telaglenastat (CB-839) can be rescued by the additional of the thiol antioxidant, N-acetylcysteine (NAC). Clonogenic cell survival assays were performed in CaSki (**E**) and SiHa PTEN$^{-/-}$ (**F**) cells 96 h after incubation with 200 nM telaglenastat (CB-839) with (CB + NAC) and without NAC rescue. *Statistical analysis:* Error bars represent ± SD of N=3 experiments performed on different days. Two tailed paired student's test was performed and asterisks represents * p <0.05. (**G-H**) *In vivo* efficacy of telaglenastat (CB-839) monotherapy in mice with (**G**) CaSki and SiHa (**H**) xenografts treated with 50 and 100 mg/Kg for 37 days. *Statistical analysis* was performed by Linear mixed model fit by REML (Restricted Maximum Likelihood). For CaSki xenograft Ctrl *vs* CB-839 50 mg/KG, Ctrl *vs* CB-839 100 mg/KG, the tumor volumes of both treated groups were smaller than Ctrl group with p<0.05. There was no significant difference between CaSki CB-839 50 mg/KG *vs* CaSki CB-839 100 mg/KG. For SiHa xenograft model Ctrl *vs* CB-839 50 mg/KG, p<0.05; Ctrl *vs* CB-839 100 mg/KG, p>0.05; CB-839 50 mg/KG *vs* CB-839 100 mg/KG, p>0.05.

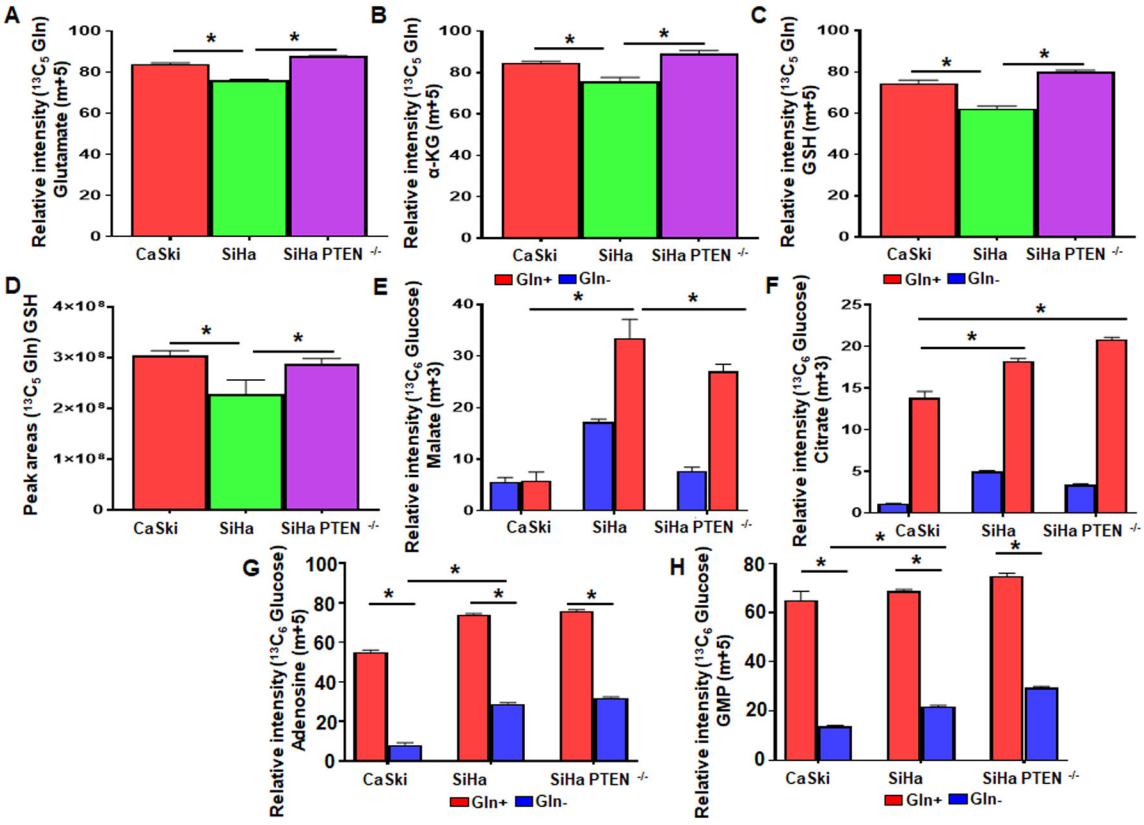

Figure 5. Stable isotope labeling demonstrates targetable outputs of glutamine metabolism in cervical cancer.

A-D Glutamine carbon is used to generate reduced glutathione (GSH) and tricarboxylic acid (TCA) cycle intermediates in PI3K activated cervical cancer cells. CaSki SiHa, and SiHa PTEN$^{-/-}$ cells were grown with $^{13}C_5$ labeled glutamine (Gln) for 18 hrs, and isotope incorporation into (**A**) glutamate (M+5 fraction), (**B**) α-ketoglutarate (α-KG M+5 fraction) and reduced glutathione (GSH represented as relative intensity of M+5 fraction (**C**) and peak areas of $^{13}C_5$Gln labeled GSH (**D**) were quantified by liquid chromatography mass spectroscopy as described in the materials and methods. **(E-F)** SiHa cells divert glucose carbon into the tricarboxylic acid cycle (TCA) intermediates under conditions of glutamine deprivation (Gln−). SiHa, SiHa PTEN$^{-/-}$ and CaSki cells were grown with $^{13}C_6$ glucose for 18hrs, followed by 48hrs of media with glutamine (Gln+) or without glutamine (Gln−), and $^{13}C_6$ glucose isotope incorporation in m+3 tricarboxylic acid (TCA) cycle intermediates (**E**) Malate and (**F**) Citrate were quantified by liquid chromatography mass spectrometry as described in the materials and methods. **(G-H)** Glutamine deprivation results in decreased generation of nucleotide precursors (**G**) adenosine and (**H**) dGMP in cervical cancer cells. *Statistical analysis:* Error bars represent ± SD of N=3 experiments performed on different days. Two tailed paired student's test was performed and asterisks represents * $p < 0.05$.

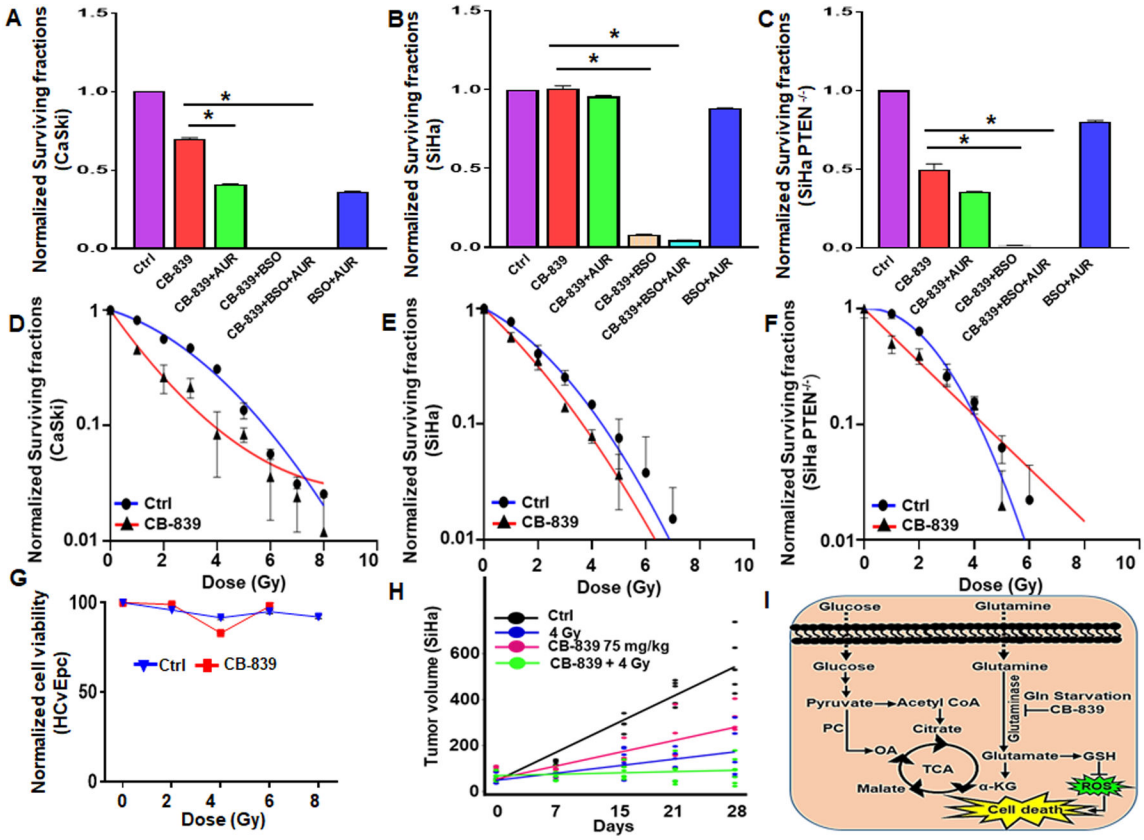

Figure 6. Pharmacologic inhibition of glutaminase can be combined with inhibitors of intracellular redox metabolism or radiation to enhance treatment efficacy-

(**A-C**) For clonogenic cell survival assays in CaSki, SiHa, and SiHa PTEN$^{-/-}$ cells were treated with 200 nM telaglenastat monotherapy (CB-839), 25 nM auranafin and 125 μM L-buthionine sulfoximine for 96h. Plating efficiencies for CaSki cells were Ctrl - 109±2, CB-839 - 76±6 , CB-839+AUR - 44±3, CB-839+BSO - 0±0.56, CB-839+BA - 0±0, BA-39±3), SiHa cells Ctrl - 130±4, CB-839 - 131±12, CB-839+AUR - 124±5, CB-839+BSO - 10±4, CB-839+BA - 6±1.5, BA - 114±4 and, SiHa PTEN$^{-/-}$ cells Ctrl - 65±3., CB-839 - 48±1.5, CB-839+AUR - 35±4, CB-839+BSO - 2±1, CB-839+BA - 2±0.5, BA- 56±3. *Statistical analysis:* Error bars represent ± SD of N=3 experiments performed on different days. Two tailed paired student's test was performed and asterisks represents * p <0.05. (**D-F**) Clonogenic cell survival assays in CaSki, SiHa, and SiHa PTEN$^{-/-}$ with CB839 (200nM) plus increasing single fraction doses of radiation. (**G**). Cell viability study of normal cervix epithelial cells HCvEpC with and without 200 nM telaglenastat (CB-839) and increasing doses of radiation. (**H**) Tumor growth delay of SiHa xenografts treated with 75mg/kg of telaglenastat (CB-839) and 4 Gy single fraction dose of tumor directed radiation delivered via SARRP. Statistical Analysis for xenograft studies was performed using Linear mixed model fit by REML (Restricted Maximum Likelihood) as described in the Materials and Methods. Ctrl *vs* 4 Gy, Ctrl *vs* CB-839, Ctrl *vs* CB-839+ 4 Gy, p<0.05; CB-839+ 4 Gy *vs* CB-839, p<0.05; 4 Gy vs CB-839+ 4 Gy p<0.05. (**I**) Schematic diagram of proposed primary mechanism of action of CB-839 in cervical cancer.